Desialylation of O-glycans on glycoprotein Ibα drives receptor signaling and platelet clearance

Yingchun Wang,[1] Wenchun Chen,[1] Wei Zhang,[2] Melissa M. Lee-Sundlov,[3] Caterina Casari,[4] Michael C. Berndt,[5] Francois Lanza,[6] Wolfgang Bergmeier,[4,7] Karin M. Hoffmeister,[3] X. Frank Zhang[2] and Renhao Li[1]

[1]Aflac Cancer and Blood Disorders Center, Children's Healthcare of Atlanta, Department of Pediatrics, Emory University School of Medicine, Atlanta, GA, USA; [2]Department of Bioengineering, Lehigh University, Bethlehem, PA, USA; [3]Blood Research Institute, BloodCenter of Wisconsin, Milwaukee, WI, USA; [4]McAllister Heart Institute, University of North Carolina, Chapel Hill, NC, USA; [5]Faculty of Health Sciences, Curtin University, Perth, Western Australia, Australia; [6]UMR_S949 INSERM, Université de Strasbourg, EFS-Alsace, Strasbourg 67065, France and [7]Department of Biochemistry and Biophysics, University of North Carolina, Chapel Hill, NC, USA

 doi:10.3324/haematol.2019.240440

Received: October 13, 2019.

Accepted: January 22, 2020.

Pre-published: January 23, 2020.

Correspondence: *RENHAO LI* - renhao.li@emory.edu

Supplement Information for

Wang et al.

Desialylation of O-glycans on glycoprotein Ibα drives receptor signaling and platelet clearance

Supplement Methods

Materials. Fluorescein isothiocyanate (FITC)-conjugated ECL, SNA and PNA and biotin-conjugated MAL-II lectins were from Vector Laboratories (Burlingame, CA). Allophycocyanin (APC)-conjugated anti-mouse CD41 (clone MWReg30), APC anti-mouse Ter-119, APC-conjugated anti-human CD41, FITC-conjugated anti-human P-selectin antibodies, and FITC-conjugated streptavidin were from Biolegend (San Diego, CA). FITC-conjugated monoclonal antibody (MAb) SZ2 was from Beckman Coulter (Brea, CA). Purified human GPIb-IX complex, MAbs WM23, 5G6, RAM.1 and GFP-LactC2 have been described.[1-4]

Filopodia assay. Fluorescence microscopy of filopodia formation was performed as described previously.[10] Briefly, washed platelets were prepared in modified Tyrode's buffer at $5x10^5$ cells. After being treated with neuraminidase or only buffer at 37˚C for 30 min, platelets were fixed with equal volume of 4% paraformaldehyde for 20 min at room temperature. Fixed platelets were placed onto an uncoated glass slide using cytospin at 1,000 rpm for 5 min and stained with 2 mg/ml TRITC-phalloidin in PBS containing 0.1% Triton X-100 for 30 min. Cell images were

acquired on a super-resolution DeltaVision OMX imaging system (GE Healthcare). Z-stack imaging was performed at 0.125 mm per step and analysis by Fiji software.

Glycan analysis by flow cytometry. To detect lectin binding in platelets, 10 μl citrated whole blood, with or without neuraminidase treatment, was incubated with 10 μl FITC-ECL (60 μg/ml), FITC-SNA (40 μg/ml) or FITC-PNA (40 μg/ml), biotin-MAL-II and FITC-streptavidin (10 μg/ml), along with 5 μg/ml APC-labeled anti-mCD41 or Ter119 antibodies at room temperature for 20 min. The samples were treated additionally by RBC lysis buffer (eBioscience, San Diego, CA). To detect binding of anti-T antigen antibodies, 10 μl citrated human or mouse PRP, with or without neuraminidase treatment, was incubated with 10 μl FITC-labeled goat anti-human IgG (2 μg/ml) or FITC-goat anti-mouse IgG (2 μg/ml), along with 5 μg/ml APC-labeled anti-hCD41 or anti-mCD41 antibodies at room temperature for 20 min. Samples were fixed by 4% paraformaldehyde and analyzed by flow cytometry. The mean fluorescence intensity was obtained for each measurement and quantitated for both platelets and erythrocytes.

Platelet aggregometry. Platelet aggregation was monitored in a dual-channel Chrono-Log aggregometer (Havertown, PA). Washed platelets were added to 2.5×10^{8} platelets/ml in a 250-µl cuvette, and Tyrode's buffer of the same volume to the control cuvette. Both were incubated for 3 min at 37˚C prior to measurement. With stirring at 1,200 rpm, the channel was calibrated for 0 to 100 % light transmission by pressing the SET BASELINES pushbutton. Aggregation was initiated by the addition of noted agonists and monitored by the change in optical density, which was converted into percentage activity over a period of 5 min.

References

1. Liang X, Russell SR, Estelle S, Jones LH, Cho S, Kahn ML, et al. Specific inhibition of ectodomain shedding of glycoprotein Ibalpha by targeting its juxtamembrane shedding cleavage site. J Thromb Haemost. 2013 Oct 5;11(12):2155-62.
2. Yan R, Mo X, Paredes AM, Dai K, Lanza F, Cruz MA, et al. Reconstitution of platelet glycoprotein Ib-IX complex in phospholipid bilayer nanodiscs. Biochemistry. 2011 Nov 14;50(49):10598-606.
3. Perrault C, Moog S, Rubinstein E, Santer M, Baas MJ, de la Salle C, et al. A novel monoclonal antibody against the extracellular domain of GPIbβ modulates vWF mediated platelet adhesion. Thromb Haemost. 2001 Nov;86(5):1238-48.
4. Berndt MC, Du XP, Booth WJ. Ristocetin-dependent reconstitution of binding of von Willebrand factor to purified human platelet membrane glycoprotein Ib-IX complex. Biochemistry. 1988 Jan 26;27(2):633-40.
5. Zhang W, Deng W, Zhou L, Xu Y, Yang W, Liang X, et al. Identification of a juxtamembrane mechanosensitive domain in the platelet mechanosensor glycoprotein Ib-IX complex. Blood. 2015 Oct 30;125(3):562-9.
6. Zhang XF, Zhang W, Quach ME, Deng W, Li R. Force-regulated refolding of the mechanosensory domain in the platelet glycoprotein Ib-IX complex. Biophys J. 2019;Epub ahead of print.

Supplement Figures legends

Figure S1. Alignment of human (top) and mouse (bottom) GPIbα sequences. Both GPIbα sequences are from UniProt (accession numbers: human P07359; mouse O35930). The sequences, including the signal sequence, are aligned with extracellular cysteines residues (colored blue) as anchors. The large gap in the alignment is mostly due to the difference in the length and the number of the tandem nucleotide repeat sequence between human and mouse orthologues. Asp residues in the N-glycosylation site motif sequence (NxT/S) are colored red, with the other Asp residues in the extracellular domain underlined. Note that while human GPIbα contains 4 potential N-glycosylation sites, including two in the N-terminal ligand-binding domain (residue number 37, 175), mouse GPIbα contains none. The closest in mouse GPIbα is residue Asn367, but it is not predicted to be glycosylated because of the proline residue that follows. Residues in the MSD are marked by dashed boxes. The blue arrowhead marks the ADAM17 shedding cleavage site in human GPIbα. The binding epitope of 5G6 is marked by the pink box. The orange line underscores the extracellular sequence (*i.e*. Trigger sequence) that is retained along with the GPIbα transmembrane and cytoplasmic domains in the IL4R-IbαTg platelet.

Figure S2. Injection of neuraminidase induces thrombocytopenia in Adam17$^{\Delta Zn/\Delta Zn}$ mice. (A) Plot of platelet counts after injection of *A. ureafaciens* α2,3,6,8-neuraminidase (10 mU per mouse) into wild-type (■) or Adam17$^{MK-/-}$ (▲) mice. Blood were collected from each mouse via facial vein immediately before (t=0) or days after the injection. Counts of platelets were performed on a cell counter and normalized with the count before the injection being 100%. Data are shown as mean±SD, n=4-6. **, $P<0.01$, by unpaired two-tailed Student's t-test. (B)

Expression levels of GPIbα in WT and Adam17$^{MK-/-}$ platelets after injection of neuraminidase, as detected by flow cytometry using a PE-conjugated anti-GPIbα antibody.

Figure S3. No IgG binding to platelets following treatment of α2,3-neuraminidase. (A) Overlaid flow cytometry histograms of binding of FITC-labeled goat anti-mouse IgG to platelets that had been treated previously with (solid red) or without (dotted gray) anti-GPIbα antibody WM23 (5μg/ml). WM23 was used here as a positive control for the extent of IgG binding to platelets. (B) Plots of change of IgG binding following α2,3-neuraminidase (α2,3-Neu) treatment of platelets. Citrated human (gray) and mouse (blue) platelets were treated with α2,3-Neu at 37˚C for 1 hr. FITC-labeled goat anti-human IgG or goat anti-mouse IgG was then added for 20 min, and the samples were fixed and analyzed by flow cytometry. The mean fluorescence intensity was measured for each cell population and normalized against that of untreated platelets (mean±SD). n.s., not significant, by unpaired two-tailed Student's t-test.

Figure S4. Thrombocytopenia at the dose of in vitro desialylation. Bacterial α2,3,6,8-neuraminidase (filled circle) or saline (open circle) was injected intravenously into wild-type mice at a dose equivalent to that used for *in vitro* treatment of platelets (same unit per ml of blood). Blood was collected from each mouse via facial vein immediately before (t=0) or after the injection. Counts of platelets were performed on a cell counter and normalized with the count before the injection being 100%. All data are shown as mean±SD, n=3.

Figure S5. Desialylation of O-glycans in purified human GPIb-IX complex following treatment of α2,3,6,8- or α2,3-neuraminidase, detected by binding of PNA lectin. Anti-

GPIbα antibody WM23 (5μg/ml) was coated to Cosato microtiter plate. Purified human GPIb-IX protein was treated with or without α2,3,6,8- or α2,3-neuraminidase at 37˚C for 1 hour. GPIb-IX was captured by immobilized WM23 and probed with lectin PNA-FITC (1:125) or antibody SZ2-HRP (1:1,500). Bound PNA was detected using anti FITC-HRP (1:500) (DAKO). All data are shown as mean±SD, n=4. n.s., not significant; ***, P<0.001, by unpaired two-tailed Student's t-test.

Figure S6. Injection of neuraminidase induces thrombocytopenia in hTg mice. α2,3-neuraminidase was injected intravenously into wild-type (■) or hTg (●) mice. Blood were collected from each mouse via facial vein immediately before (t=0) or days after the injection. Counts of platelets were performed on a cell counter and normalized with the count before the injection being 100%. Data are shown as mean±SD, n=4-6. **, $P<0.01$, by unpaired two-tailed Student's t-test.

Figure S7. St3gal1$^{MK-/-}$ platelets display more constitutive filopodia than WT. Citrated washed murine WT and St3gal1$^{MK-/-}$ platelets were collected, fixed by paraformaldehyde, stained with phalloidin, and imaged by confocal fluorescence microscopy. (A) Representative images of WT and St3gal1$^{MK-/-}$ platelets. The right panel is a close-up of a platelet with filopodia (white arrow). Scale bar, 10 μm. (B) Quantification of filopodia in WT and St3gal1$^{MK-/-}$ platelets. The percentage of filopodia+ platelets from 16 view fields were visually examined and counted. Data are shown as mean±SD. ***, $P<0.001$, by unpaired two-tailed Student's t-test.

Figure S1. Mouse GPIba does not contain any N-glycosylation sites.

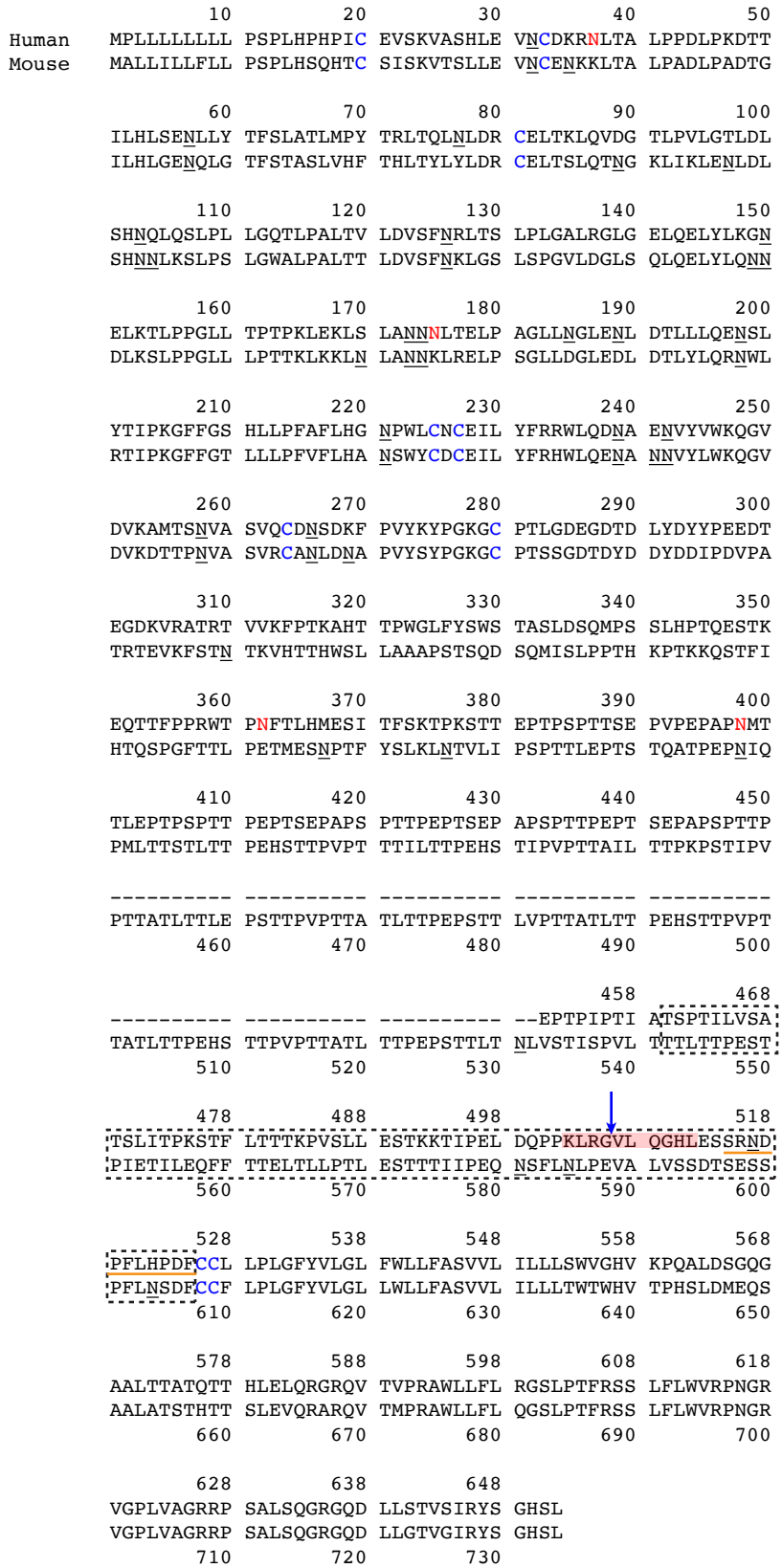

Figure S2. Neuraminidase causes platelet clearance in Adam17$^{MK-/-}$ mice

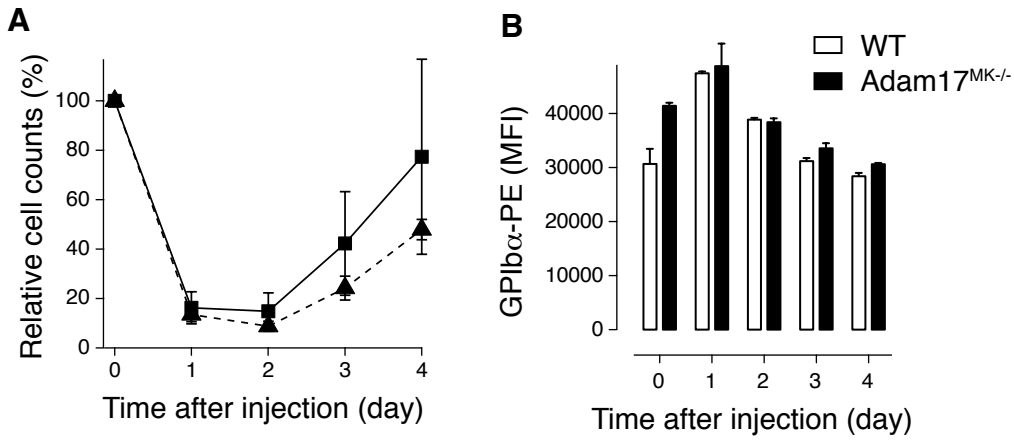

Fig S3. Little IgG binding to desialylated platelets

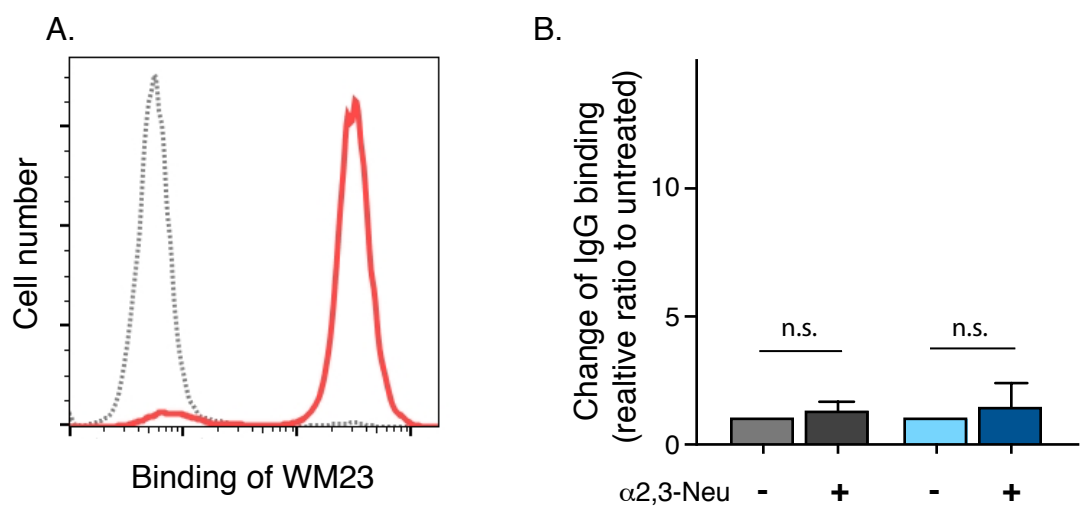

Fig S4. Neuraminidase induces thrombocytopenia in hours

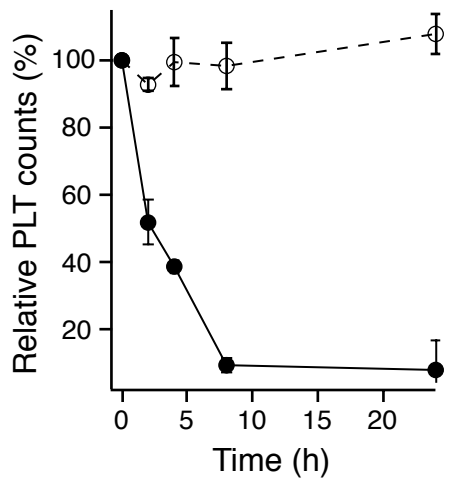

Figure S6. Neuraminidase causes platelet clearance in hTg mice

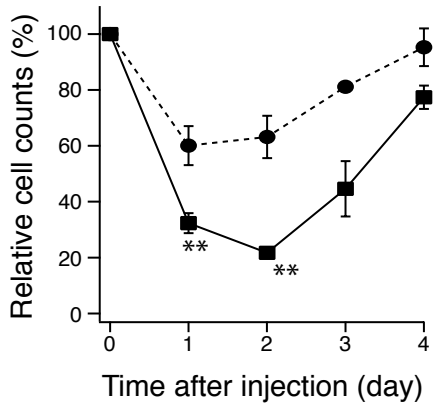

Fig S5. Desialylation of O-glycans in purified GPIb-IX complex

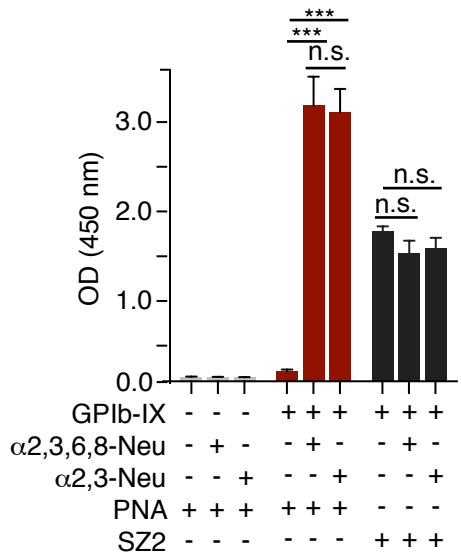

Fig S7. Upregulated GPIb-IX signaling in St3gal1$^{MK-/-}$